Molecular Dynamics Simulations of *Trichomonas vaginalis* Ferredoxin Show a Loop-Cap Transition

Tiffany E. Weksberg,* Gillian C. Lynch,† Kurt L. Krause,†‡§ and B. Montgomery Pettitt*†
*Structural and Computational Biology and Molecular Biophysics, Baylor College of Medicine, Houston, Texas 77030;
†Department of Chemistry and ‡Department of Biology and Biochemistry, University of Houston, Houston, Texas, 77004;
and §Department of Biochemistry, University of Otago, Dunedin, New Zealand 9001

ABSTRACT The crystal structure of the oxidized *Trichomonas vaginalis* ferredoxin (Tvfd) showed a unique crevice that exposed the redox center. Here we have examined the dynamics and solvation of the active site of Tvfd using molecular dynamics simulations of both the reduced and oxidized states. The oxidized simulation stays true to the crystal form with a heavy atom root mean-squared deviation of 2 Å. However, within the reduced simulation of Tvfd a profound loop-cap transition into the redox center occurred within 6-ns of the start of the simulation and remained open throughout the rest of the 20-ns simulation. This large opening seen in the simulations supports the hypothesis that the exceptionally fast electron transfer rate between Tvfd and the drug metronidazole is due to the increased access of the antibiotic to the redox center of the protein and not due to the reduction potential.

INTRODUCTION

Trichomonas vaginalis is a sexually transmitted protozoan that causes the disease trichomoniasis. With an estimated 5 million new cases occurring in 1998, *T. vaginalis* is one of the most common sexually transmitted infections in the United States (1). *T. vaginalis* is pervasive and cases are often asymptomatic. Fortunately, infections are usually curable with a single dose of the drug metronidazole, a nitroimidazole (trade name Flagyl). *T. vaginalis* has recently come under closer scrutiny, as studies have shown that infection can increase the transmission rate of human immunodeficiency virus (HIV) (2–5). This fact, coupled with the often subclinical nature of an infection, points to *T. vaginalis* as an important public health risk. In addition, there is an increasing prevalence of metronidazole-resistant *T. vaginalis* strains (6).

For more than 30 years, *T. vaginalis* has proven to be an excellent organism to use to study the mechanism of action of the important antibiotic metronidazole. *T. vaginalis*' exquisite sensitivity to metronidazole sparked extensive research in the 1980s that uncovered an important role of hydrogenosomal ferredoxin in the activation of this prodrug. Within *T. vaginalis*, the hydrogenosomal protein *T. vaginalis* ferredoxin (Tvfd) activates the drug metronidazole. Tvfd is a small protein at 9.8 kD and 93 residues with a [2Fe-2S] cluster that participates in electron transfer reactions (7). Physiologically, Tvfd functions to shuttle electrons between pyruvate:ferredoxin oxidoreductase and hydrogenase in the metabolic cycle of *T. vaginalis* (8). When metronidazole is present, an electron is transferred from Tvfd to the drug. Interestingly, Tvfd has a redox potential of −347 mV, which is more positive than photosynthetic [2Fe-2S] ferredoxins (e.g., −440 mV for vegetative Anabaena ferredoxin) (9) but less positive than most oxidase ferredoxins. Unfortunately, no cocrystal with both Tvfd and metronidazole exists.

The crystal structure for this protein was solved to 2.2 Å by x-ray crystallography (10). Overall, the fold was similar to that found for [2Fe-2S] vegetative and oxidase classes of ferredoxins. The average B-factors from the crystal structure were 35, 36, and 47 $Å^2$, respectively, for the three molecules A, B, and C in the asymmetric unit (10). In addition, electron density for the third molecule in the asymmetric unit showed main chain breaks between residues 31 and 42 (10), and all molecules showed increased B-factors for this loop of residues, >80 $Å^2$ for Asp-35 (Protein Data Bank structure 1L5P). These data suggested to us that the [2Fe-2S] active site loop was dynamic and that one of the molecules of Tvfd in the unit cell might have a different structural conformation for the loop than the other two molecules of Tvfd in the asymmetric unit. Since strict noncrystallographic symmetry restraints were used in the solution of the structures, no variations would have been seen between the backbones of the molecules in the crystal structure (10). Few waters in the interior of the protein and none within 6 Å of the active site were resolved (10). The crystal structure revealed an interesting feature of Tvfd: one side of the iron-sulfur cluster was more exposed to solvent than other similar ferredoxin structures, with a small cavity allowing one of the active site sulfurs to be just accessible. These results prompted the hypothesis that direct access to the active site cluster was responsible for the fast kinetic rates seen for the Tvfd to metronidazole electron transfer reaction: first, from the crystal structure showing an opening into the active site (10) and second, from the kinetic data that showed extremely fast metronidazole active by Tvfd (11).

The exact role of Tvfd in metronidazole activation is an object of debate and continued study. Tvfd has been found to activate metronidazole in a variety of different experiments.

Submitted April 27, 2006, and accepted for publication November 27, 2006.
Address reprint requests to B. Montgomery Pettitt, E-mail: pettitt@uh.edu.

0006-3495/07/05/3337/09 $2.00
doi: 10.1529/biophysj.106.088096

Work carried out in vitro showed rapid activation of metronidazole by Tvfd (11), and some studies have also shown lowered expression of Tvfd mRNA in metronidazole-resistant strains of *T. vaginalis* (12). Expression of Tvfd in a metronidazole-resistant *Trichomonas fetus* cell line that was lacking native ferredoxin expression lead to metronidazole susceptibility within the cell line (13). In addition, kinetic studies of the ferredoxin to nitroimidazole electron transfer reaction showed that Tvfd reduces metronidazole and other nitroimidizole drugs one to two orders of magnitude faster than [2Fe-2S] photosynthetic *Anabaena* ferredoxin, even given that the *Anabaena* ferredoxin has a more negative redox potential (11).

Interestingly, however, a Tvfd knockout was created that did not show resistance to metronidazole, leading to the hypothesis that there may be other ferredoxins or flavins in *T. vaginalis* in addition to Tvfd that can activate the drug (14). Review of the recently completed Tvfd genome reveals seven hydrogenosome targeted ferredoxin genes (15), explaining why a single knockout would be unlikely to result in nitroimidazole resistance. Although these other redox proteins may play a role, the preponderance of evidence points to Tvfd as a major activation protein of metronidazole in *T. vaginalis*.

The two iron atoms in plant-type ferredoxins are high spin, antiferromagnetically coupled to each other (16). Preceding the reaction with metronidazole, the [2Fe-2S] cluster in Tvfd is in its reduced state, Fe^{+2}/Fe^{+3}. The extra electron was shown in plant-type ferredoxins to be localized to the iron closest to the exterior of the protein (labeled Fe1) by NMR spectroscopy using the nuclear Overhauser effect (17). The iron sulfur site is coordinated with the protein through the sulfur groups on four cysteines (7). Three of these cysteines are part of a loop of residues 31–48 that wraps around the iron-sulfur cluster shielding it from the solvent. In the process of antibiotic activation, an electron is transferred from the reaction center to metronidazole, oxidizing the [2Fe-2S] cluster. Once the electron is transferred to metronidazole, electron spin resonance studies show a characteristic nitro radical species for metronidazole (18–22). This radical anionic species of metronidazole causes oxidative damage to the organism, mainly through inhibition of nucleic acid synthesis (23) caused by direct damage to DNA (18,24). Although metronidazole has a redox potential of −345 mV, comparable to many ferredoxins from anaerobes, it is more negative than most aerobes. Various mechanisms are postulated for metronidazole being used to treat human anaerobic infections without damaging human DNA such as the redox potential difference of TvFd verses aerobes reduction potentials and metronidazole (14) or by oxygen inactivation of metronidazole radicals (25).

Two [2Fe-2S] ferredoxins have been crystallized in both their reduced and oxidized forms. *Anabaena* ferredoxin structures differed by a flip of the backbone between Cys-46 and Ser-47 (26). Those authors labeled the flip ''CO out'' in the reduced form and ''CO in'' in the oxidized form. There were no other structural changes between the two forms of the protein. Putidaredoxin has also been crystallized in the reduced form and compared to the oxidized x-ray crystal structures (27). The reduced form also showed an analogous backbone flip, between Cys-45 and Ala-46. In addition, other small structural changes were seen within the region of the iron-sulfur cluster.

In this study we set out to explore the role of flexibility in the [2Fe-2S] loop region of the protein and its potential implications in metronidazole activation. We hypothesize that the structural flexibility in the loop composed of residues 31–48 and the additional access to the active site sulfur seen in the crystal structure may play a role. Since no cocrystal has been solved, we look solely at the dynamics of the Tvfd protein. Starting with the crystal structure of Tvfd solved to 2.2 Å by multiple anomalous dispersion phasing (10), we explore the dynamics of solvation and the structure of the active site region to better explain Tvfd's exceptionally fast kinetics and selective activation of metronidazole. We use molecular dynamics (MD) simulations to study the movement and solvation of a model of Tvfd. Two simulations of equal length were performed, one with the protein in the reduced state, and the other in the oxidized state. These simulations were run for a period of time (20 ns) sufficient to observe aspects of conformational equilibrium in the protein.

MATERIALS AND METHODS

The all-atom force field employed was the Charmm27 potential (28). Because the iron-sulfur parameters were not included as part of the Charmm27 set, they were derived from experimental and computational sources. The bond and angle force constants were obtained from resonance Raman spectra (29), the partial charges from density functional calculations (30), and the angles and dihedrals from those used in the refinement of the crystal structure (10). Other ferredoxin simulation studies have used the force constants from similar sources (31,32).

The initial configuration was the structure labeled A in the asymmetric unit from the crystal structure of Tvfd (1L5P), but with added hydrogens. This structure was chosen as it had the lowest average B-factor and the best electron density throughout the main chain (10). The protein was solvated with 9447 Charmm TIP3P water (33) molecules within a cubic box of length 66.4 Å. No water was placed for which the oxygen from the water was within 2.5 Å of a heavy atom in the protein. This setup produced at least three solvation shells around the protein. Nine sodium counterions were added to the box to neutralize the charge on the protein, and an additional 32 Na^+ and 32 Cl^- were added to make a final salt concentration of 0.18 molar NaCl. The ions were added by replacing a water molecule randomly in the box. The same box was used to set up the oxidized structure; however, the appropriate parameters were used and a sodium ion was removed to neutralize the charge in the box. This initial box went through three rounds of steepest decent minimization: the first round minimized the water holding the protein rigid, the second minimized the protein while holding the water rigid, and the third minimized the whole system.

MD simulations were run using the microcanonical ensemble with periodic boundary conditions in the Extended System Program (34). Electrostatics were calculated using the Ewald sum (35), with the Lennard-Jones real space cutoff set to 16.2 Å. Ewald parameters were optimized using the guidelines set by Fincham (36) with rcut set to 16.2 Å. The RATTLE algorithm (37) was used to constrain all the bond lengths with a tolerance of 1×10^{-7} Å, and the Velocity Verlet algorithm was utilized with a time step

of 2 femtoseconds. The system was initially relaxed by running a series of 10 10-ps simulations with velocities being reassigned at increasing intervals. Another 900 ps of simulation was run with no modifications during equilibration.

All root mean-squared deviation (RMSD) and dihedral calculations were calculated using visual molecular dynamics (VMD) (38). Water and ion density profiles were calculated by dividing the simulation box into 81 bins per side of the box, which translates to a bin length of 0.82 Å. The oxygen nucleus in a water molecule was used to form the water density histograms. This was done over the last nanosecond of trajectory data and normalized (39). The same calculation was done for ions. The system was equilibrated for 1 ns as described above. After equilibration, 20 ns of production were run with trajectory snapshots saved every 100 femtoseconds. The total energy of the two simulations after equilibration remained constant; both had an internal root mean-squared difference of <0.956 kcal/mol.

RESULTS

Overall behavior of the oxidized state simulation

Directly after equilibration, the RMSD for the heavy atoms in the oxidized state trajectory and the crystal structure increased from 1.5 Å to 2 Å and stayed at 2 Å RMSD for the rest of the simulation (Fig. 1). This is well within acceptable limits and was expected as the crystal structure was produced from the protein in the oxidized state (10). Mean-squared atomic fluctuation (MSF) showed strong variations with respect to different time windows. These calculations were done for the 3rd, the 10th, and the 19th nanosecond of trajectory data and also compared to the B-factors for each molecule in the asymmetric unit of the crystal (10) (Fig. 2). The time periods over which the trajectories were averaged for later comparison were chosen for having stable equilibrated structures over at least an entire nanosecond of data. They correspond to a time period after a conformational change that also includes relaxation time for the other molecules in the system to respond to the protein's changes. From this point on, the time

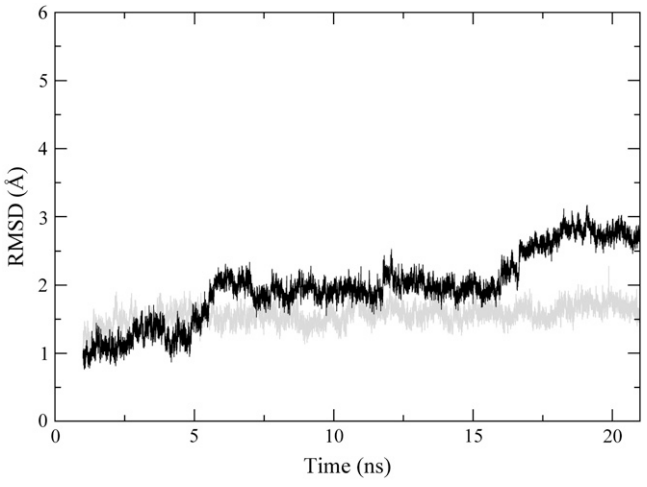

FIGURE 1 RMSD between the crystal structure C-α atoms and the C-α atoms in the reduced state trajectory (*solid*) and the oxidized trajectory (*shaded*).

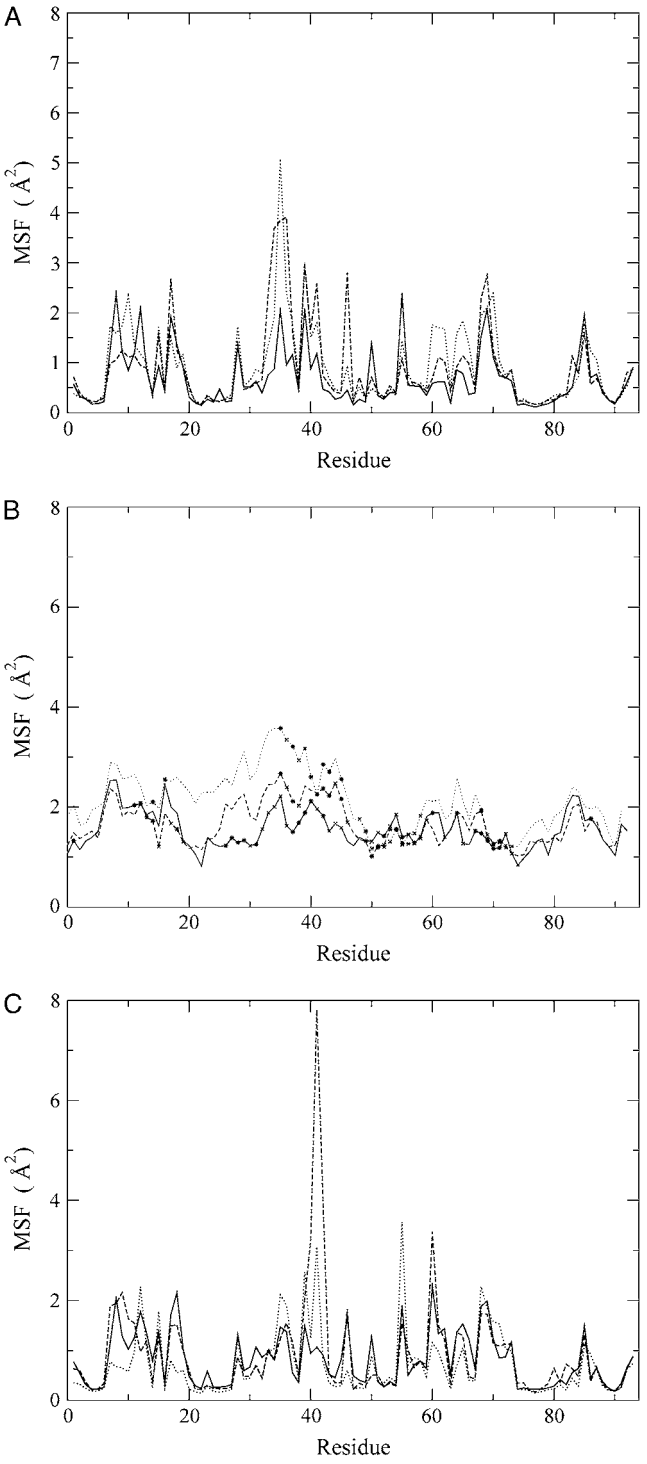

FIGURE 2 (*A*) MSF calculations for the oxidized simulation over the 3rd nanosecond (*solid*), the 10th nanosecond (*dashed*), and the 19th nanosecond (*dotted*). (*B*) Scaled B-factors for each molecule in the asymmetric unit of the crystal; molecule A (*solid*), molecule B (*dashed*), molecule C (*dotted*) (10), residues with crystal contacts within 4 Å are denoted *, residues within 6 Å are denoted x (40). (*C*) MSF calculations for the reduced simulation over the 3rd nanosecond (*solid*), the 10th nanosecond (*dashed*), and the 19th nanosecond (*dotted*).

period before the 5th nanosecond will be labeled T1, the 5th nanosecond to the 15th nanosecond labeled T2, and the time period after the 15th nanosecond T3. Also, averaged structures over the 3rd, 10th, and 19th nanoseconds will be labeled S1, S2, and S3, accordingly. The calculations were completed over 1-ns windows to provide enough data to represent the local minimum surface.

The MSF was calculated for each individual residue by first aligning all trajectory structures in a nanosecond of trajectory data with the averaged structure from the time period. The RMSD was then taken between each residue in the averaged structure and each trajectory structure residue; these were then averaged for each residue over the full nanosecond. Previous analyses have shown that mean-squared residue fluctuations can be related to experimental x-ray crystallography B-factors by multiplying the B-factor with $(3/8\pi^2)$ (40).

Although it is difficult to quantitatively relate the B-factors to the MSF calculations due to errors in the model, non-crystallographic restraints in the refinement, and poor density in some regions (10), a clear relation between the two is seen in the trends of each graph. The differences in MSF between the different nanoseconds calculated showed only small differences in the fluctuations occurring in the residues, which indicate stability. There are, however, small changes that have occurred in the structure that were seen from the backbone overlay of three averaged structures and the crystal structure (Fig. 3). Some movement in the loop composed of residues 31–48 that contains the active site was seen. Examination of the crystal contacts in the crystal structure (Fig. 2 *B*) shows contacts in the loop region for all molecules. However, molecule A has more than C, and B has more than C (41). This could be one explanation for the improved order of the loop in molecule A in comparison to B and C. Note that B and C are quite similar to A in the rest of the protein (not the loop) despite having fewer contacts.

Overall behavior of the reduced state simulation

During the reduced simulation a striking conformational transition occurred: a new opening to the active site was revealed (Fig. 4). The RMSD between each structure in the trajectory including equilibration was calculated against the crystal structure for heavy atoms and for the C-α atoms. The major feature of this opening event was seen in the increase in heavy atom RMSD from <2 Å to >2.5 Å at the fifth nanosecond (Fig. 1).

The most obvious change seen upon comparison of S1 and S2 is a large conformational transition in the loop at residues 31–49 (Fig. 5), which contains three of the cysteines coordinated to the [2Fe-2S] cluster, whereas the rest of the protein showed typical low structural deviations. When the heavy atom RMSD of just this loop, residues 31–49, was calculated against the same residues in the starting crystal structure a 4.5-Å RMSD was seen, whereas there was no significant change seen in the RMSD of the protein excluding the loop (Fig. 6). This dynamic loop is in the same region where there were experimental crystal structure

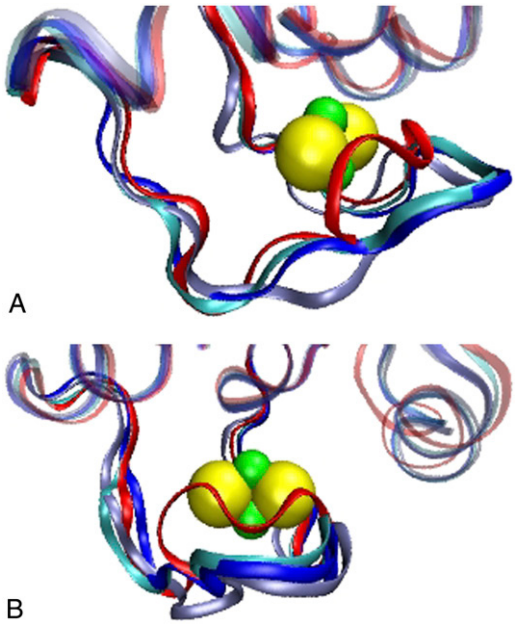

FIGURE 3 Backbone overlay of the crystal structure (*red*) with the averaged structures of the oxidized simulation from the 3rd (*dark blue*), 10th (*blue*), and 19th (*light blue*) nanosecond with *A* and *B* rotated 90°.

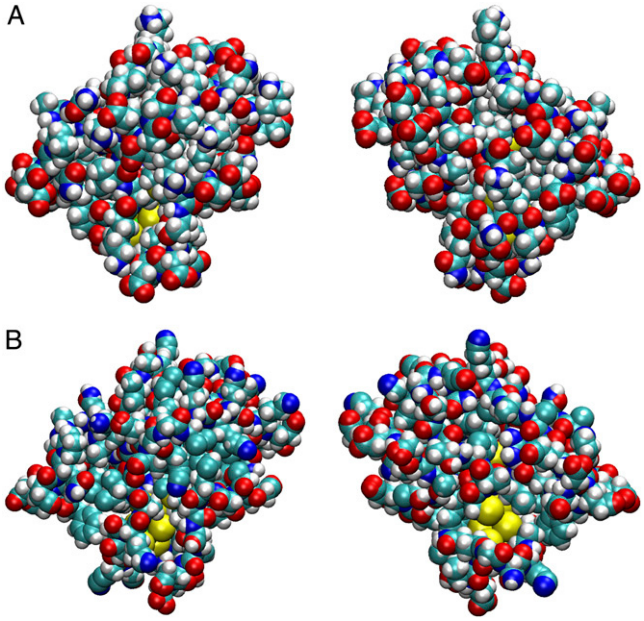

FIGURE 4 Van der Waals representation of (*A*) the crystal structure and (*B*) the S2 reduced simulation structure. Carbon atoms are cyan, hydrogens are white, oxygen is red, nitrogen is blue, and sulfur is yellow. The redox site is located at the bottom of the figure. Left and right structures are rotated 180°.

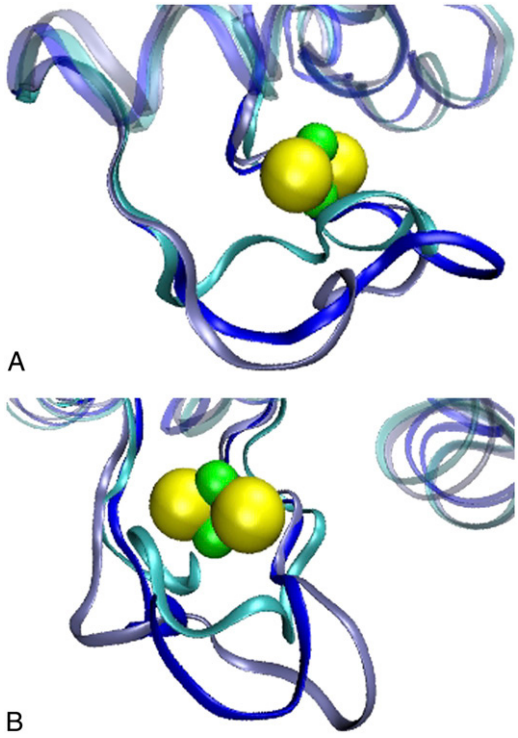

FIGURE 5 Backbones of structures S1 (*cyan*), S2 (*blue*), and S3 (*light blue*) from the reduced simulation. Loop residues 31–49 are opaque, whereas the rest of the protein is transparent. The [2Fe-2S] cluster is in green and yellow. *A* and *B* are rotated 180° of each other.

refinement difficulties in one of the three monomers found in the asymmetric unit (10). It is the deviation from the crystal structure of this loop portion of the protein that increases the heavy atom RMSD, whereas the rest of the protein is essentially stable. When viewing the loop in S1 and S2, the top and edge of the loop that was originally tilted up

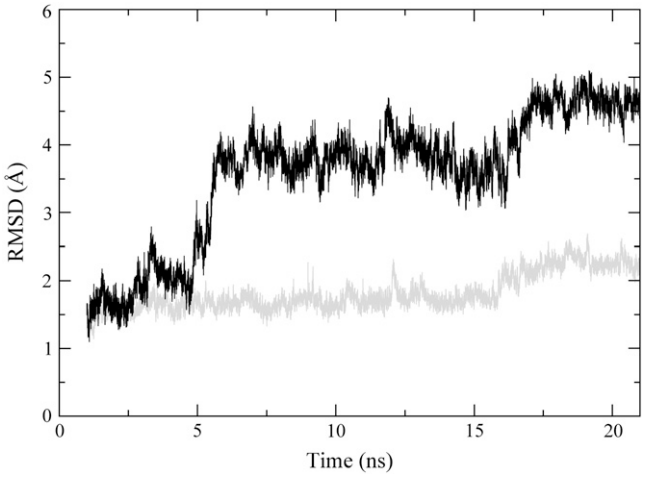

FIGURE 6 RMSD between the crystal structure heavy atoms and heavy atoms in the reduced simulation trajectory; for residues 31–47 (*solid*), for all residues except 31–47 (*shaded*).

shielding the [2Fe-2S] cluster has moved away from the cluster and is instead extended into the solvent region, leaving a sizable accessible pocket near the [2Fe-2S] cluster. This provides different and larger access to the iron sulfur cluster than seen in the crystal structure. There are two areas in the structures of S2 and S3 that deviate. The first is the same loop as between S1 and S2 made of residues 31–49; the second is between residues 81–89, in which the third helix in the protein has relaxed. Dynamically, the iron-sulfur cluster moves very little and has an RMSD compared to the crystal structure after the loop movement of 0.85 Å.

For our simulation, the mean-square fluctuations were calculated independently for S1, S2, and S3 (Fig. 2 *C*). Our calculation showed high fluctuations in residues 31–49, which also showed increased experimental B-factors (Fig. 2 *B*). In addition, during T3 the fluctuations of residues 81–89 increase, which matches the higher B-factors in the crystallographic data for this region. Although there are some difficulties relating to the direct correlation between these two graphs as discussed earlier, the MSF showed the same trends as the crystallographic B-factors, but with a more dynamic active site loop.

Analysis of loop-cap opening transition

The conformational change during the fifth nanosecond of simulation occurred over ~1 ns. The first step in this structural change was seen at 4.8 ns, during which the dihedral angles of Lys-42 and Ala-43 flip (Fig. 7). At 5.4 ns on the opposite side of the loop, residues 34–39 move away from the [2Fe-2S] cluster. This loop movement was also observed in the dihedral angles of Ala-34, Asp-35, Asp-36, and Gln-39 (Fig. 7). Further movement of the loop occurs after the 16th nanosecond to move the tip of the loop farther from the protein close to 90° from where it was originally located in the crystal structure, further enlarging the exposure of the [2Fe-2S] cluster. This was shown in the additional dihedral movements of Gln-39 and Lys-42 near the end of the simulation (Fig. 7).

In addition to movement in the protein, the water density profile in this region changed concomitantly during the fifth nanosecond. In the T1 structure, water density was observed in distinct regions near the active site, whereas in the T2 structure there was a broad area of high water density located far into the newly opened crevice (Fig. 8). When looking at the structures' trajectory over T2, the water in the crevice was very dynamic, moving quickly into and out of the active site crevice with low residence times.

The ions in this simulation also experience changes in their residence times and location because of this conformational change. Before the loop opening, the ions stayed mostly in the bulk water with some ions having a high residence time near oppositely charged solvent exposed residues on the surface of the protein. During the next 5 ns of simulation, ions moved in and out of the newly exposed iron

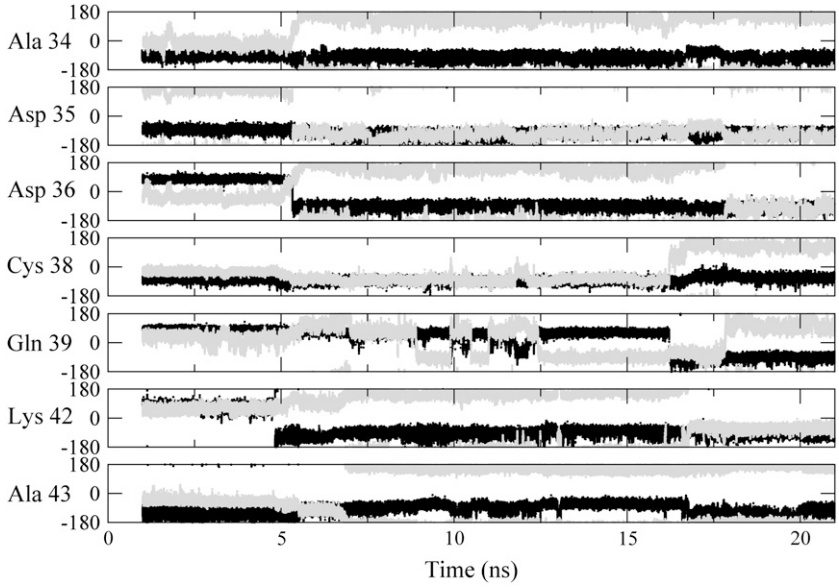

FIGURE 7 Dihedral angles φ (*solid*) and ψ (*shaded*) of specific residues in the active site loop.

cluster active site crevice, with a sodium ion displaying a long time residence near the sulfur atoms by Fe1 of the [2Fe-2S] cluster. Fe1 is the iron closest to the exterior of the protein; it is located closest to the bottom of all the figures in this work.

The nonbonded interactions between the protein and the [2Fe-2S] cluster changed significantly after the fifth nanosecond. The movement of the loop away from the iron-sulfur cluster disturbed many of the nonbonded interactions between the backbone of the protein and the cluster. In addition, a structurally significant salt link was broken; this interaction was between Lys-42 and Glu-65. This connection ''held'' the top of the loop closed against the second helix in the structure which was not directly connected to the redox cluster. As the loop moved away from the cluster, the noncovalent bond was broken between this pair, with the residues then becoming solvated. The analysis of the dynamics of the active site during the fifth nanosecond showed that residues 31–49 have opened up to create a crevice that is large enough to allow easy access to the [2Fe-2S] cluster to both dynamic water and ions.

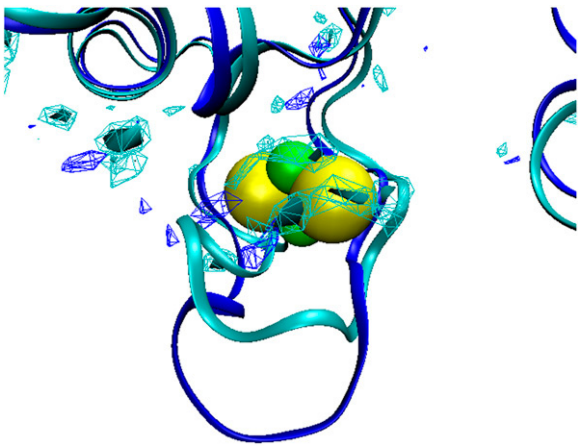

FIGURE 8 Water density profiles calculated over a nanosecond for both S1 (*cyan*) and S2 (*blue*) overlaid on the respective protein backbone. Meshed regions indicate high water density (>0.094 $Å^{-3}$), solid density regions indicate very high water density (>0.141 $Å^{-3}$). Bulk density (not shown) was 0.035 $Å^{-3}$. The iron-sulfur cluster is shown in yellow and green.

DISCUSSION

Our two simulations have provided insight into the dynamics and function of the Tvfd protein. The loop that was closed over the iron-sulfur cluster in the crystal structure has moved out from the active site in the reduced state simulation and created a new wide crevice allowing access to the [2Fe-2S] cluster, which was seen to a much lesser degree in the oxidized simulation. In addition, in the reduced state the dynamics of the water changed from exhibiting high residence times near the original iron-sulfur crevice to being very mobile in the same region after the loop-cap transition. The conformational change in the reduced structure occurs very early in the simulation, with the structure remaining in the loop-open conformation for the majority of the simulation. This suggests that the conformational change is significant and not a transient sampling of conformational space. Also, the fluctuations of the individual residues relaxed over both simulations to give a closer agreement to the B-factors from the crystallographic data, with the oxidized simulation matching the B-factors much closer than those of the reduced simulation. This was to be expected as the crystal structure was obtained with the protein in the oxidized state (10). This loop-cap transition seen to a lesser extent in the oxidized state can also explain the refinement difficulties in this region for the original x-ray data; it implies

conformational heterogeneity in the structure. It is known that redox centers of metalloproteins can undergo photoreduction during synchrotron data collection (42,43). It is possible that this phenomenon could have occurred during the data collection for the structure; but no direct proof is available.

Computational studies on both the reduced and oxidized states of a rubredoxin have also shown increased solvation of the active site in the reduced state in relation to the oxidized state (44). In addition, loop-cap transitions of this type have been described before. In triosephosphate isomerase a loop-cap transition plays a key kinetic role in the mechanism (45). Studies on the oxidized and reduced state of both *Anabaena* ferredoxin (26) and putidaredoxin (27) showed that conformational changes near the active site have occurred between the two redox states. This implies loop movement near the redox center is associated with redox state.

Marcus and Sutin showed that the electron transfer rate is dependent on the coupling between the electron acceptor and donor, which is mainly due to distance, the redox potential, and the so-called rearrangement energy cost of the reaction (46). If the electrostatic thermodynamic driving force were the main contribution to the electron transfer rate (47), then *Anabaena* ferredoxin would be expected to show faster kinetics than Tvfd due to its higher reducing potential, −440 mV for *Anabaena* ferredoxin versus −347 mV for Tvfd. However, this is not the case, implying that either the electronic coupling or the rearrangement energy must be the primary determining factor of the kinetic rate.

The crystal structure of Tvfd showed a crevice in Tvfd that modestly exposes the iron-sulfur cluster of the active site to solution (10). Our simulation showed a different but nearby large active site exposure in the reduced state through the movement of the active site loop away from the iron-sulfur cluster. This clearly allows for molecular contact with solvent and small molecule drugs like metronidazole. A distance decrease of 20 Å between reacting centers has been previously shown to increase to 10^{12} in the electron transfer rate (48). Interestingly, it has also been theoretically shown that the solvation of iron-sulfur clusters may also affect the redox potential, with more highly solvated clusters having a more positive redox potential (49). Although we cannot make direct comparisons with kinetics from just this one simulation, we can hypothesize that the opening of the loop of residues to create an opening into the active site would allow metronidazole easier access to the [2Fe-2S] cluster, and thereby faster reaction kinetics.

The structural changes shown here also give a plausible explanation of the experimental crystal B-factor data. This is an indication that the experimental density that was seen in the structure was related to the actual dynamics of the protein. Our simulation also predicts that changes to certain amino acids in the protein will affect the kinetics. Changes to Lys-42 and Asp-62 or Glu-65 should affect the kinetics since this nonbonded link may keep the loop closed. In addition, other residues could be changed within the [2Fe-2S] binding region to investigate steric affects. We hope to test these hypotheses in future work.

Due to both the increase in drug-resistant strains and to the link between Trichomoniasis and increased HIV transmission rates, *T. vaginalis* is a serious public health risk. Greater understanding of the mechanism of current therapy can aid efforts to counteremerging resistance as well as aid in our understanding of electron transfer reactions of high relevance to biology. To this end, our results have shown a loop-cap transition that not only explains the high B-factors seen in the crystallographic data, but also offers an explanation of the exceptionally fast and selective electron transfer kinetics seen for Tvfd and nitroimidazoles.

SUPPLEMENTARY MATERIAL

An online supplement to this article can be found by visiting BJ Online at http://www.biophysj.org.

The authors are grateful for support from the National Institutes of Health, the Robert A. Welch Foundation, and a training fellowship from the Keck Center for Computational and Structural Biology of the Gulf Coast Consortia (NLM grant No. 5T15LM07093). This research was performed in part using the MSCF in EMSL, a national scientific user facility sponsored by the U.S. Department of Energy OBER and located at PNNL. This research was also supported by the National Science Foundation through TeraGrid resources provided by SDSC, PSC, and NCSA.

The authors acknowledge the use of VMD for making the molecular graphics plots and CCP4 for calculation of the crystal contacts in Fig. 2.

REFERENCES

1. Alexander, L. L., J. R. Cates, N. Herndon, and J. F. Ratcliffe. 1998. Sexually Transmitted Diseases in America: How Many and at What Cost? American Social Health Association. December, 1998.
2. Laga, M., A. Manoka, M. Kivuvu, B. Malele, M. Tuliza, N. Nzila, J. Goeman, F. Behets, V. Batter, M. Alary, and others. 1993. Non-ulcerative sexually transmitted diseases as risk factors for HIV-1 transmission in women: results from a cohort study. *AIDS*. 7:95–102.
3. Hobbs, M. M., P. Kazembe, A. W. Reed, W. C. Miller, E. Nkata, D. Zimba, C. C. Daly, H. Chakraborty, M. S. Cohen, and I. Hoffman. 1999. *Trichomonas vaginalis* as a cause of urethritis in Malawian men. *Sex. Transm. Dis.* 26:381–387.
4. Sorvillo, F., L. Smith, P. Kerndt, and L. Ash. 2001. *Trichomonas vaginalis*, HIV, and African-Americans. *Emerg. Infect. Dis.* 7:927–932.
5. Nusbaum, M. R., R. R. Wallace, L. M. Slatt, and E. C. Kondrad. 2004. Sexually transmitted infections and increased risk of co-infection with human immunodeficiency virus. *J. Am. Osteopath. Assoc.* 104: 527–535.
6. Upcroft, P., and J. A. Upcroft. 2001. Drug targets and mechanisms of resistance in the anaerobic protozoa. *Clin. Microbiol. Rev.* 14:150–164.
7. Johnson, P. J., C. E. d'Oliveira, T. E. Gorrell, and M. Müller. 1990. Molecular analysis of the hydrogenosomal ferredoxin of the anaerobic protist *Trichomonas vaginalis*. *Proc. Natl. Acad. Sci. USA*. 87:6097–6101.
8. Kulda, J. 1999. Trichomonads, hydrogenosomes and drug resistance. *Int. J. Parasitol.* 29:199–212.
9. Vidakovic, M. S., G. Fraczkiewicz, and J. P. Germanas. 1996. Expression and spectroscopic characterization of the hydrogenosomal

[2Fe-2S] ferredoxin from the protozoan *Trichomonas vaginalis*. *J. Biol. Chem.* 271:14734–14739.

10. Crossnoe, C. R., J. P. Germanas, P. LeMagueres, G. Mustata, and K. L. Krause. 2002. The crystal structure of *Trichomonas vaginalis* ferredoxin provides insight into metronidazole activation. *J. Mol. Biol.* 318:503–518.
11. Vidakovic, M., C. R. Crossnoe, C. Neidre, K. Kim, K. L. Krause, and J. P. Germanas. 2003. Reactivity of reduced [2Fe-2S] ferredoxins parallels host susceptibility to nitroimidazoles. *Antimicrob. Agents Chemother.* 47:302–308.
12. Quon, D. V. K., C. E. d'Oliveira, and P. J. Johnson. 1992. Reduced transcription of the ferredoxin gene in metronidazole-resistant *Trichomonas vaginalis*. *Proc. Natl. Acad. Sci. USA.* 89:4402–4406.
13. Land, K. M., M. G. Delgadillo, and P. J. Johnson. 2002. In vivo expression of ferredoxin in a drug resistant trichomonad increases metronidazole susceptibility. *Mol. Biochem. Parasitol.* 121:153–157.
14. Land, K. M., M. G. Delgadillo-Correa, J. Tachezy, S. Vanacova, C. L. Hsieh, R. Sutak, and P. J. Johnson. 2004. Targeted gene replacement of a ferredoxin gene in *Trichomonas vaginalis* does not lead to metronidazole resistance. *Mol. Microbiol.* 51:115–122.
15. Carlton, J. M., R. P. Hirt, J. C. Silva, A. L. Delcher, M. Schatz, Q. Zhao, J. R. Wortman, S. L. Bidwell, U. C. Alsmark, S. Besteiro, T. Sicheritz-Ponten, C. J. Noel, J. B. Dacks, P. G. Foster, C. Simillion, Y. Van de Peer, D. Miranda-Saavedra, G. J. Barton, G. D. Westrop, S. Muller, D. Dessi, P. L. Fiori, Q. Ren, I. Paulsen, H. Zhang, F. D. Bastida-Corcuera, A. Simoes-Barbosa, M. T. Brown, R. D. Hayes, M. Mukherjee, C. Y. Okumura, R. Schneider, A. J. Smith, S. Vanacova, M. Villalvazo, B. J. Haas, M. Pertea, T. V. Feldblyum, T. R. Utterback, C. L. Shu, K. Osoegawa, P. J. de Jong, I. Hrdy, L. Horvathova, Z. Zubacova, P. Dolezal, S. B. Malik, J. M. Logsdon Jr., K. Henze, A. Gupta, C. C. Wang, R. L. Dunne, J. A. Upcroft, P. Upcroft, O. White, S. L. Salzberg, P. Tang, C. H. Chiu, Y. S. Lee, T. M. Embley, G. H. Coombs, J. C. Mottram, J. Tachezy, C. M. Fraser-Liggett, and P. J. Johnson. 2007. Draft genome sequence of the sexually transmitted pathogen *Trichomonas vaginalis*. *Science.* 315:207–212.
16. Dunham, W. R., G. Palmer, R. H. Sands, and A. J. Bearden. 1971. On the structure of the iron-sulfur complex in the two-iron ferredoxins. *Biochim. Biophys. Acta.* 253:373–384.
17. Dugad, L. B., G. N. La Mar, L. Banci, and I. Bertini. 1990. Identification of localized redox states in plant-type two-iron ferredoxins using the nuclear Overhauser effect. *Biochemistry.* 29:2263–2271.
18. Moreno, S. N., R. P. Mason, R. P. Muniz, F. S. Cruz, and R. Docampo. 1983. Generation of free radicals from metronidazole and other nitroimidazoles by *Tritriichomonas foetus*. *J. Biol. Chem.* 258:4051–4054.
19. Moreno, S. N., R. P. Mason, and R. Docampo. 1984. Distinct reduction of nitrofurans and metronidazole to free radical metabolites by *Tritrichomonas foetus* hydrogenosomal and cytosolic enzymes. *J. Biol. Chem.* 259:8252–8259.
20. Willson, R. L., B. C. Gilbert, P. D. Marshall, and R. O. Norman. 1974. Metronidazole ('Flagyl'): a pulse radiolysis and e.s.r. study. *Int. J. Radiat. Biol.* 26:427–434.
21. Moore, D. E., C. F. Chignell, R. H. Sik, and A. G. Motten. 1986. Generation of radical anions from metronidazole, misonidazole and azathioprine by photoreduction in the presence of EDTA. *Int. J. Radiat. Biol.* 50:885–891.
22. Whillans, D. W., and G. E. Adams. 1975. Electron-affinic sensitization VI: a pulse radiolysis and ESR comparison of some 2- and 5-nitroimidazoles. *Radiat. Res.* 62:407–421.
23. Ings, R. M., J. A. McFadzean, and W. E. Ormerod. 1974. The mode of action of metronidazole in *Trichomonas vaginalis* and other microorganisms. *Biochem. Pharmacol.* 23:1421–1429.
24. Willson, R. L., W. A. Cramp, and R. M. Ings. 1974. Metronidazole ('Flagyl'): mechanisms of radiosensitization. *Int. J. Radiat. Biol. Relat. Stud. Phys. Chem. Med.* 26:557–569.
25. Müller, M., and T. E. Gorrell. 1983. Metabolism and metronidazole uptake in Trichomonas vaginalis isolates with different metronidazole susceptibilities. *Antimicrob. Agents Chemother.* 24:667–673.
26. Morales, R., M. H. Charon, G. Hudry-Clergeon, Y. Pétillot, S. Norager, M. Medina, and M. Frey. 1999. Refined x-ray structures of the oxidized, at 1.3 Å, and reduced, at 1.17 Å, [2Fe-2S] ferredoxin from the cyanobacterium *Anabaena* PCC7119 show redox-linked conformational changes. *Biochemistry.* 38:15764–15773.
27. Sevrioukova, I. F. 2005. Redox-dependent structural reorganization in putidaredoxin, a vertebrate-type [2Fe-2S] ferredoxin from *Pseudomonas putida*. *J. Mol. Biol.* 347:607–621.
28. MacKerell, A. D. Jr., D. Bashford, M. Bellott, R. L. Dunbrack Jr., J. D. Evanseck, M. J. Field, S. Fischer, J. Gao, H. Guo, S. Ha, D. Joseph-McCarthy, L. Kuchnir, K. Kuczera, F. T. K. Lau, C. Mattos, S. Michnick, T. Ngo, D. T. Nguyen, B. Prodhom, W. E. Reiher III, B. Roux, M. S. Schlenkrich, J. C. Smith, R. Stote, J. Straub, M. Watanabe, J. Wiórkiewicz-Kuczera, D. Yin, and M. Karplus. 1998. All-atom empirical potential for molecular modeling and dynamics studies of proteins. *J. Phys. Chem. B.* 102:3586–3616.
29. Yachandra, V. K., J. Hare, A. Gewirth, R. S. Czernuszewicz, T. Kimura, R. H. Holm, and T. G. Spiro. 1983. Resonance Raman spectra of spinach ferredoxin and adrenodoxin and of analogue complexes. *J. Am. Chem. Soc.* 105:6462–6468.
30. Mouesca, J.-M., C. L. Jun, L. Noodleman, D. Bashford, and D. A. Case. 1994. Density functional/Poisson-Boltzmann caulculations of redox potentials for iron-sulfur clusters. *J. Am. Chem. Soc.* 116:11898–11914.
31. Dolan, E. A., R. B. Yelle, B. W. Beck, J. T. Fischer, and T. Ichiye. 2004. Protein control of electron transfer rates via polarization: molecular dynamics studies of rubredoxin. *Biophys. J.* 86:2030–2036.
32. Roitberg, A. E. 1997. A molecular dynamics study of Fe2S2 putidaredoxin: multiple conformations of the C-terminal region. *Biophys. J.* 73:2138–2148.
33. Jorgensen, W. L., J. Chandrasekhar, and J. D. Madura. 1983. Comparison of simple potential functions for simulation liquid water. *J. Chem. Phys.* 79:926–935.
34. Pettitt, B. M. 1996. ESP: Extended System Program. Developed in the Research Laboratory of Prof. B. M. Pettitt at the University of Houston, Houston, TX.
35. de Leeuw, S. W., J. W. Perram, and E. R. Smith. 1980. Simulation of electrostatic systems in periodic boundary conditions. I. Lattice sums and dielectric constants. *Proc. R. Soc. Lond. A.* 373:27–56.
36. Fincham, D. 1994. Optimization of the Ewald sum for large systems. *Mol. Simul.* 13:1–9.
37. Andersen, H. C. 1983. RATTLE: a velocity version of the shake algorithm for molecular dynamics calculations. *J. Comput. Phys.* 52: 24–34.
38. Humphrey, W., A. Dalke, and K. Schulten. 1996. VMD: visual molecular dynamics. *J. Mol. Graph.* 14:33–38.
39. Makarov, V., B. M. Pettitt, and M. Feig. 2002. Solvation and hydration of proteins and nucleic acids: a theoretical view of simulation and experiment. *Acc. Chem. Res.* 35:376–384.
40. Brooks, C. L., M. Karplus, and B. M. Pettitt. 1988. Proteins: A Theoretical Perspective of Dynamics, Structure, and Thermodynamics. John Wiley & Sons, New York.
41. Krissinel, E., and K. Henrick. 2005. Detection of protein assemblies in crystals. *CompLife.* 2005:163–174.
42. Alphey, M. S., M. Gabrielsen, E. Micossi, G. A. Leonard, S. M. McSweeney, R. B. Ravelli, E. Tetaud, A. H. Fairlamb, C. S. Bond, and W. N. Hunter. 2003. Tryparedoxins from *Crithidia fasciculata* and *Trypanosoma brucei*: photoreduction of the redox disulfide using synchrotron radiation and evidence for a conformational switch implicated in function. *J. Biol. Chem.* 278:25919–25925.
43. Roberts, B. R., Z. A. Wood, T. J. Jonsson, L. B. Poole, and P. A. Karplus. 2005. Oxidized and synchrotron cleaved structures of the disulfide redox center in the N-terminal domain of *Salmonella typhimurium* AhpF. *Protein Sci.* 14:2414–2420.
44. Yelle, R. B., N. S. Park, and T. Ichiye. 1995. Molecular dynamics simulations of rubredoxin from *Clostridium pasteurianum*: changes in structure and electrostatic potential during redox reactions. *Proteins.* 22:154–167.

45. Joseph, D., G. A. Petsko, and M. Karplus. 1990. Anatomy of a conformational change: hinged ''lid'' motion of the triosephosphate isomerase loop. *Science*. 249:1425–1428.

46. Marcus, R. A., and N. Sutin. 1985. Electron transfers in chemistry and biology. *Biochim. Biophys. Acta*. 811:265–322.

47. Meyer, T. E., C. T. Przysiecki, J. A. Watkins, A. Bhattacharyya, R. P. Simondsen, M. A. Cusanovich, and G. Tollin. 1983. Correlation between rate constant for reduction and redox potential as a basis for systematic investigation of reaction mechanisms of electron transfer proteins. *Proc. Natl. Acad. Sci. USA*. 80:6740–6744.

48. Moser, C. C., J. M. Keske, K. Warncke, R. S. Farid, and P. L. Dutton. 1992. Nature of biological electron transfer. *Nature*. 355: 796–802.

49. Kassner, R. J., and W. Yang. 1977. A theoretical model for the effects of solvent and protein dielectric on the redox potentials of iron-sulfur clusters. *J. Am. Chem. Soc*. 99:4351–4355.